**Biogeosciences
Discussions**

Fractal metrology for biogeosystems analysis

V. Torres-Argüelles[1], K. Oleschko[2], A. M. Tarquis[3], G. Korvin[4], C. Gaona[2],
J.-F. Parrot[5], and E. Ventura-Ramos[1]

[1]Universidad Autónoma de Querétaro, Querétaro, México
[2]Centro de Geociencias, Universidad Nacional Autónoma de México (UNAM), Blvd. Juriquilla
3001, Qro., 76220, Querétaro, México
[3]Dep. of Applied Mathematics to Agricultural Engineering (E.T.S.I.A.) C.E.I.G.R.A.M.,
Technical University of Madrid (U.P.M.), Ciudad Universitaria, 28040, Madrid, Spain
[4]King Fahd University of Petroleum and Minerals, Dhahran 31261, Saudi Arabia
[5]Instituto de Geografía, UNAM, Ciudad Universitaria, D.F., México

BGD

7, 4749–4799, 2010

**Fractal metrology for
biogeosystems
analysis**

V. Torres-Argüelles et al.

Title Page

Abstract	Introduction
Conclusions	References
Tables	Figures

Back | Close

Full Screen / Esc

Printer-friendly Version

Interactive Discussion

Abstract

The solid-pore distribution pattern plays an important role in soil functioning being related with the main physical, chemical and biological multiscale and multitemporal processes. In the present research, this pattern is extracted from the digital images of three soils (*Chernozem, Solonetz* and *"Chocolate" Clay*) and compared in terms of roughness of the gray-intensity distribution (the measurand) quantified by several measurement techniques. Special attention was paid to the uncertainty of each of them and to the measurement function which best fits to the experimental results. Some of the applied techniques are known as classical in the fractal context (box-counting, rescaling-range and wavelets analyses, etc.) while the others have been recently developed by our Group. The combination of all these techniques, coming from Fractal Geometry, Metrology, Informatics, Probability Theory and Statistics is termed in this paper *Fractal Metrology* (FM). We show the usefulness of FM through a case study of soil physical and chemical degradation applying the selected toolbox to describe and compare the main structural attributes of three porous media with contrasting structure but similar clay mineralogy dominated by montmorillonites.

1 Introduction

"If you cannot measure it you cannot manage it" (Cox, 2002). If you cannot measure something with known exactness and precision you cannot make unbiased decisions. The science of measurements is called *Metrology* and it deals with the theoretical and practical aspects of measurements (ISO, 2004; JCGM, 2008). The main goal for Metrology is to outline ways in which metrological constants can be measured to required accuracies (NIST, 2001). To date, some nine well-defined disciplines have developed from the original Metrology, each one focusing on specific objectives (Fig. 1), with several emerging areas in the development phase (such as *Roughness Metrology,* Villarubia, 2005). Uncertainty and bias are the scopes of *Statistical Metrology*

V. Torres-Argüelles et al.

Full Screen / Esc

(Willink, 2005; Cox et al., 2008), while the features which affect the reliability of the measurements of linear and angular quantities in industrial production are analyzed by *Dimensional Metrology* (Curtis and Farago, 2007). The structure of uncertainty is analyzed in a reference way by Working Group 1 of the Joint Committee for Guides in Metrology (JCGM/WG1). We suggest that the study of complex and deeply interconnected *Biogeosystems*, whose behavior is defined by a common principle of self-organizing criticality (Beiró et al., 2008), requires special measurands (quantities to be measured, ISO, 2004) and a corresponding toolbox of reference measurement techniques to quantify scale invariance (SI), universality (UNI), nonlinearity (NL), complexity (COM), criticality (CR) as well as the uncertainty of their measurements. The lack of reference techniques, standards and quality control for the measurements of these basic attributes of complex systems, makes difficult any intergroup comparisons of the usually extensive data surveys, resulting in unsustainable decision-making. In this study, we combine some principles and techniques of *Fractal Geometry*, *Metrology*, *Informatics*, *Probability Theory* and *Statistics* inside a new branch of Metrology, called *Fractal Metrology*, and introduce *scale invariant roughness* as the main measurand of SI, UN, COM and CR of complex systems (Oleschko et al., 2008).

The present study has three goals: (i) To validate the step-by-step protocol for measuring the scale invariance of roughness on the structural patterns of a complex system (*soil* in our case), paying special attention to the uncertainty of each used measurement technique; (ii) To test some new (designed by our group), as well as some common roughness measurement techniques on three soils with contrasting structural patterns, but with the same reference-mineralogy; (iii) To compare qualitatively (by visualization) and a quantitatively (in terms of the Hurst exponent) the symmetry breaking of soil aggregates under a degradation process (sodium salinization).

2 Complexity, criticality and roughness

We designed *Fractal Metrology* to measure the degree of complexity and criticality of complex biogeosystems in terms of the roughness (main measurand) of their structural patterns. Under *complexity*, following Christensen and Moloney (2005), we understand the phenomenon when "the repeated application of simple rules in systems with many degrees of freedom gives rise to emergent behavior not encoded in the rules themselves". In the present research this behavior was observed during the collapse of the solid and pore patterns of *Chernozem* under a common agricultural degradation process, salinization, leading to an emergent new unfertile soil, namely *Solonetz*. The structural pattern of the later is compared with the pure "Chocolate" Clay (a kind of clayey deposits in Russia with chocolate color) composed by minerals of the montmorillonite group. The main difference between these soils is the origin of the dominating cation inside the CEC (Cation Exchange Complex): calcium is dominating in the Calcic Chernozem, while sodium prevails in Solonetz and Chocolate Clay. The Solonetz was formed from the Chernozem inside the same Chernozem-Solonetz pedological complex (Oleschko, 1981), while the Chocolate Clay was taken as the example of a reference-matrix which has never been involved in the aggregation process (Vadyunina et al., 1980).

The term *criticality* refers to the behavior of the system at the point of phase transition, where no characteristic scale exists (and therefore there is pure scale invariance, Christensen and Moloney, 2005). In the present study we are looking for critical behavior in the Chernozem-Solonetz complex, comparing the soil structural patterns before and after the transition from the totally aggregated (State I, Chernozem) to massive (State II, Solonetz) structure (Oleschko, 1981). During this transition, the structural pattern of Chernozem, a highly fertile soil with perfectly permeable sponge structure (Fig. 3a) gets transformed into the massive structure (Fig. 3c) of the unfertile bad land (Solonetz). Note that these two soils were located inside a surface mosaic only a few meters from each other. In the present study we focus our attention on those main

structural attributes of Chernozem which have remained unchanged during the transition to Solonetz, and test the ability of Fractal Metrology to measure the differences or similarities between the compared soils.

Roughness is a basic common feature of all kinds of either real-world systems (natural, social, economical or technological) or mathematics. Weisstein (2010), in agreement with Finch (2001, 2003) defines a k-rough (or k-jagged) number as a positive integer whose prime factors are all greater than or equal to k. In the real-world, roughness characterization is mostly limited to visual judgment. The surface roughness appears as a set of apparently random peaks and valleys, resulting in the fine-texture irregularities due to the interaction of internal and external processes (El-Sonbaty et al., 2008). Smooth surfaces are rare in Nature (Majumdar and Bhushan, 1991), while rough ones have many useful properties ("*rough skin is good*" for suppressing air turbulence, see Monroe, 2006; Fransson et al., 2006). Roughness has a considerable effect on the contact of surfaces (Borri-Brunetto et al., 1999); it can influence *adhesion* (Wang et al., 2008), *friction* (Kim et al., 2006), *wear* (Bigerelle et al., 2007), and *reflection* (Verhoest et al., 2008). While surface roughness has a positive effect in increasing adhesion it is considered as an undesirable imperfection from the point of view of friction (Chandrasekaran and Sundararajan, 2004; Jensen, 2006). In each of the above-mentioned examples a small change in the distribution of heights, widths, or curvatures of the peaks has an important effect on the rough surface's behavior (Kim et al., 2006). Light scattering from optical coatings is the best example for how strongly processes could be affected by the roughness of interfaces (Germer, 2000). However, in spite of the great influence of surface roughness on system behavior its measurement is still a notable problem of Metrology (Villarubia, 2005; Van Gorp et al., 2007). Therefore, a quantitative measurement of surface roughness is essential for several applied and theoretical fields (Diehl and Holm, 2006), and would be especially useful in Biogeosciences. The question is: how to measure roughness in reference mode? We propose to extract the roughness from bi-dimensional digital images, time series and signals by methods suitable for box-counting and scale invariance analyses.

3 Fractals and scale invariance

No formal definition of fractals exists. Informally, Mandelbrot (2002) defines the fractals as irregular shapes, in either mathematics or the real world, with the property that each small part of them is a reduced-size copy of the whole. Mandelbrot emphasizes that the use of words *fracture* and *fractal* derived from the same root (*fractus*) is not a mere accident. First by Mandelbrot et al. (1984), and then by numerous follow-up studies, it has been shown that the fractal dimension D (the main distinctive attribute of a fractal) is an invariant measure of the roughness of fractures in metals and rocks (Mandelbrot, 2002). Mandelbrot proposed to view *Fractal Geometry* as a scientific approach to describe the sensation of rough versus smooth, as a "study of scale invariant roughness". Fractal Metrology has the same goal and measurand but it focuses on the selection and calibration of reference measurement techniques and their comparison in terms of uncertainty, as well as the best fitting measurement model.

Spatio-temporal invariance which is a main feature of natural nets and the basic concept of Physics is especially suitable to describe the structural patterns of complex systems. At present, the four most widely used types of spatial invariance in Physics (Nambu, 2008) are rotational invariance (ferromagnets); translational invariance (crystals); local gauge invariance (superconductors); and, global gauge invariance (superfluids). Recently, *scale invariance* as well has been found useful in applied sciences and for theoretical purposes.

We propose the scale invariant roughness as the main measurand of Fractal Metrology. Mandelbrot (2002, 5–6) argued that "*much in nature is ruled by what used to be called pathology*" but, fortunately, the latter "*is not unmanageable*". He continued: "*This is so because it obeys a form of invariance or symmetry that overlaps Nature and Mathematics, and is called scale invariance or scaling that is central to my life work... The challenge is to explain why so many rough facets of Nature are scale-invariant.*" At this step, we define the main goal of Fractal Metrology as the pass from *roughness sensation* to *quantitative measure* (in agreement with Mandelbrot, 2002) by introducing

the metrological measurand, selection of the corresponding reference measuring tools and assignment of a realistic uncertainty to the measurements (compared by Student's-*t* and Pearson's *r* correlation analyses). This way, we shall accomplish the three main tasks of Metrology (NIST, 2001).

3.1 Optics of fractal objects

Surface reflectance properties are among the most important attributes of matter. Recognizing the material from these properties (such as lightness and gloss) is a nontrivial task (Fleming et al., 2003), being related with problems of the "universe of projections" (Puente, 2004). The reflectance measurements by a scanning optical microscope proved to be statistically effective to inspect the surfaces of optical components for imperfections (ranging from sub-micrometer to several micrometres, Gomez et al., 1998). Fleming et al. (2003) documented that a skewed distribution of illuminant intensities is a necessary condition for perceiving surface reflectance, as the skew tends to increase the contrast between darkest and brightest regions. Korvin (2005) generalized Pentland's (1984) result about the fractal dimension of the optical image of rough surfaces. He proved, without imposing the condition that the reflection obeys Lambert's Law, that the surface and the image have the same fractal dimension and therefore the roughness can be statistically extracted from the images. We designed two methods to extract the digital image roughness, by converting the original image consisting of $N_r \times N_c$ pixels to a time series (.*ts*). Every pixel has a gray value p_{ij} between 0 and 255. Here $i = 1, \ldots, N_r$ is the row-index, $j = 1, \ldots, N_c$ is the column index, where N_r and N_c depend on the image size (mean image size in the present research was 1000×874). One way to convert an image to a time series is to rearrange all pixels row-wise into a 1-dimensional (1-D) array $F = \{p_{11}, p_{12}, \ldots, p_{1N}, p_{21}, \ldots p_{2N}, \ldots, p_{N1}, \ldots p_{NN}\}$ of length 1000×874, what we call *firmagram* (Oleschko et al., 2004) and whose roughness can be measured by algorithms available for the analysis of self-affine sets. Another possibility is to consider the *empirical histogram* $n_k = \{\#(p_{ij} = k \mid k = 0, 1, \ldots, 255)\}$,

or its normalized version, the *empirical PDF* $p_k = \left\{ \frac{n_k}{N^2} \,\middle|\, k=0,1,\ldots,255 \right\}$. The series $p_1, p_2, \ldots, p_{255}$, extracted from each digital image of interest constitutes the time series for further fractal analysis. Note that by definition a stochastic process (or random function $\{x(t)\}_\alpha$) is a family of real- (or complex-) valued functions depending on a random parameter α, where t usually plays the role of time. In the case of images analysis t represents the pixel position (in case of *firmagram* analysis) or pixel value (in case of *PDF* analysis).

4   Metrology

While as Hardy (1940) observed, a mathematician makes patterns, the specialist in Metrology should make these patterns workable. Metrology is the science looking for the specific theoretical and practical aspects of the measurement and traceability, uncertainty and calibration carried out in the numerous applied and theoretical fields (JCGM, 2008). It was born to make comparisons based on quantitative measurements and directed to understand, interpret and make correct decisions about the system of interest. The selection of measurand is the first step in each measuring process. When this selection is made keeping in mind the strict standards of Metrology, the objects or system measurements become statistically precise and close to the true values of parameters.

5   Fractal metrology

Complex systems exhibit scaling properties which obey power laws (Katz, 2006; Plowman et al., 2007). In spite of the above-mentioned diversity of the branches of Metrology (Fig. 1), two main features of complex systems – scale invariance and spontaneous symmetry breaking (Brink, 2008) – are still not measurable by standardized quantities (measurands) and reference measurement techniques. In a search for the

general (and probably universal) principles underlying the internal structure and external behavior of such systems it is indispensable to develop a generic pattern-oriented framework based on metrological principles and suitable for the measurement of complexity (Grimm et al., 2005). This framework should provide a unifying scheme for the main definitions, notions and techniques. The standardization however, is by no means a trivial procedure (Berry, 2001).

5.1 Basic concepts of fractal metrology

The metrological description of each phenomena of interest comprises certain clearly defined steps (JCGM, 2008). The present research focuses on three of them: 1. The selection of the main measurand; 2. The comparison in terms of uncertainty between the known techniques for measurand quantification; 3. The selection of measurement model for measurements representation. These steps are visualized on Fig. 2. The image of a tree (*Mezquite* from Queretaro State, Mexico) was used as to represent the branching structure (Dodds, 2010) of the information required by Fractal Metrology. This tree forms the base of the hierarchical ordering, clustering, coding, switching and control in a Fractal Metrology network of elements (Kaneko, 1990). This graph is suitable to design the step-by-step procedure for measurement of scale invariant roughness of multiscale and multitemporal images, time series or signals. The distinctive feature of this information organization and management is a clear hierarchical and logical character of the system functioning. Three main roots are constituted by data banks which alimented the highly ramified branches (consisting of by known and new measurement techniques) through the unique trunk corresponding to the dimensionless measurands of roughness (fractal dimensions and corresponding Hurst exponents). The uncertainty is taken as the main indicator of efficiency of each compared technique to quantify the measurand with known precision. The Weierstrass-Mandelbrot function is selected to represent analytically the measurement function that fits well to experimental measurements of scale invariant roughness. This way of analysis ensures optimal interaction among all elements of the net, putting in evidence "why leaves

aren't trees" (Monroe, 2010).

5.1.1 Hurst exponent as the measurand

We selected the Hurst exponent as the main measurand of roughness and therefore of Fractal Metrology, because of its ability to express the asymptotic statistical proper-
ties of a random process $x(t)$ (Denisov, 1998), and because it merges local and global features of space/time anisotropy inside the unique variable called *roughness*. Pro-
posed by the hydrologist Harold Edwin Hurst (1951), the classical rescaled adjusted range R/S-statistics have become a popular and robust technique for local and global dependence analysis (Mandelbrot, 2002). In time-series the Hurst exponent measures
the growth of the standardized range of the partial sum of deviations of a data set from its mean (Ellis, 2007). Mandelbrot and Wallis (1968) have incorporated in the Hurst methodology ordinary least squares (OLS) regression techniques, and proposed to estimate the statistics over several subseries (windows) dividing the whole series length (Ellis, 2007). The Hurst exponent (H) is related to the fractal dimension (D) by
a simple (conjectured) rule, that first time appeared in Hardy's (1916) work:

$$D = 2 - H, \tag{1}$$

where 2 is the Euclidean dimension of the space where the fractal is embedded. The Hurst exponent is especially suitable to characterize *stochastic processes* (Mandelbrot and van Ness, 1968) from the point of view of scale invariance (Bassler et al., 2006).
There are basic differences between *persistent* ($H > 0.5$) and *antipersistent* ($H < 0.5$) processes, while the white noise is characterized by $H = 0.5$. Note that the H values tend to 0 when the roughness is growing.

5.2 "Toolbox" of fractal metrology

The soil roughness was extracted from digital images and measured on firmagram,
histogram and probability density function by selected measurement techniques.

5.2.1 Firmagram roughness

Image digitization refers to the transformation of an apparently continuous image into discrete intensity values distributed at equally spaced locations across an *xy*-grid, called a *raster* (Pawley, 2006). The procedure results in an array of rows and columns which we (Oleschko et al., 2004) proposed to analyze as a one-dimensional array of data gathered inside the same column. The graphical representation of this column is the above-mentioned firmagram (Oleschko et al., 2004). The whole distribution of gray-tones (from 0 – black, to 255 – white) inside an image represents its global roughness (Fig. 4Ab, Bb, Cb), while a baseline of each selected area refers to the local roughness. This dual representation visualizes how the image roughness is changing with scale, with an accuracy of one pixel. The Histo_Gene algorithm (Parrot, 2003) scans the image from the first pixel on the top line until the final one on the bottom, building a column of the intensity values. The output files are in *.ts* format therefore the measurement of their roughness becomes a trivial task (see *measurement techniques*).

5.2.2 Histogram roughness

The second way to extract the measurand for our research is using the histogram. The histogram is considered a precise way to summarize the statistical information associated with a complex system (Strauss, 2009; Tancrez et al., 2009). To get the histogram in the present work we used the algorithm *Frequ_Hist*, written by Parrot (2003). The *Frequ_Hist* output file consists of the frequencies of occurrence (y) of each gray-intensity value (x), forming a time series whose roughness can be measured by selected reference techniques. The output file of the *Hist_Gene* (*.ts*) is transferred to *Frequ_Hist* (*.xls*). The output file of the latter algorithm consists of four data columns. The first one contains the values of gray tones extracted from the original gray-scale image, arranged in decreasing order. The second one displays the frequency of each gray scale value. These two columns correspond to the histogram constructed with the precision of one pixel. The third and forth columns correspond to the gray value and

respective probability to find it inside the image, constituting the *effective probability density function* (PDF$_{ef}$) of the analyzed image (Fig. 4Ad, Bd, Cd). The roughness of both PDFs is quantified by the measurement techniques (see Sect. 5.3). The PDF$_{ef}$ is compared with the modeled theoretical distribution by means of the @RISK (Palisade Corporation, 2005) software (Fig. 4Ae, Be, Ce).

5.2.3 Probability density function roughness

The Histogram is one of the most useful forms of summarizing random data for visual and statistical analysis (Lu and Guan, 2009). It is an extremely useful tool for graphically represent data variability which is described in quantitative terms by the *probability density function* (Strauss, 2009). For a continuous function, the PDF expresses the probability that the variable of interest X lies in an interval $(a\ b)$, (see, e.g. NIST/SEMANTECH, 2006):

$$\int_a^b f(x)dx = \Pr[a \leq X \leq b].$$

For a discrete distribution, the PDF represents the probability that the variable X takes the value x. Note, that when displayed, the PDF graph has the same appearance as the histogram (Fig. 4Ad, Bd, Cd, Fig. 4Ae, Be, Ce).

Berry (1996) was first who drew attention to "some unexpected fractal properties" of the probability density

$$P(r,t) \equiv |\Psi(r,t)|^2 \, (r = \{x_1, x_2, \ldots x_D\})$$

for what he called "the simplest imaginable nonstationary Schrödinger wave Ψ". He proved that the discordance in the initial and boundary conditions in a D-dimensional box B, enforcing an initial discontinuity at the walls, making superposition $\Psi(r,t)$ a fractal function in time and space (Berry, 1996). He computed the plan view of the roughness of the fractal probability density landscape $P(\xi, \tau)$ in time and space. For the

fractals in fractal boxes he has suggested some simple modifications which give D_{time} and D_{space}.

In our research the fractal behavior of PDF was found empirically. In addition to the PDF estimation by means of *Frequ_Hist*, the statistical analysis of the gray-tone distribution across each analyzed image has also been accomplished by the commercial software @RISK 4.5 add-in for Microsoft Excel (Palisade Corporation, 2005). The tools of *Risk Analysis* have been used since long for the analysis of financial data oscillations, but rarely applied in Natural Sciences. We have found @RISK a user-friendly software (except its rather high price!) suitable for Biogeoscience studies because of its precision and relative simplicity.

The @RISK 4.5 package selects the best fit to the experimental data function from among 37 different theoretical probability distributions (Normal, Lognormal, Logistic, Beta, Gamma, Pareto, etc.). The algorithm is based on a Monte-Carlo simulation technique which replaces the uncertain or unknown values of an experimental dataset by a range of more probable values. The list of five selected, best fitting functions are displayed automatically, the first one being the most probable for the studied data. To create a histogram, the software finds the maximum and minimum values of a data range, divides the range into classes whose level of importance depends on the probability of occurrence of values, defined as $\{p\}=\{p_1,p_2,\ldots,p_n\}$=data rank array. In @RISK 4.5 (Palisade Corporation, 2005) the probability density function is used to construct the frequency distribution from an infinitely large set of values where the class size is becoming infinitesimally small. The visual similarity between PDFs constructed by *Frequ_Hist* and @RISK can be observed in Fig. 4Ad, Bd, Cd and Ae, Be, Ce.

5.3 Measurement techniques

There are a legion of fractal descriptors suitable to quantify the specific attributes of complex systems. For instance, the fractal dimension (D) measures the set's space-filling ability (Mandelbrot, 1982); the degree of its *translation invariance* is quantified by *lacunarity* Λ (Pendleton et al., 2005; Feagin, 2003; Feagin et al. 2007); the continuity

Title Page

Abstract | Introduction

Conclusions | References

Tables | Figures

◄ | ►►

◄ | ►

Back | Close

Full Screen / Esc

Printer-friendly Version

Interactive Discussion

and tortuosity of the pore and solid networks are measured by *random-walk fractal dimensions* (Korvin, 1992; Rodriguez-Iturbe and Rinaldo, 1997), or *spectral dimension* or *fracton* (Orbach, 1986). The main advantages and problems of fractal descriptor measurements have been described in details in some by now standard (Korvin, 1992; Barton and La Pointe, 1995; Falconer, 1997; Turcotte, 1997, etc.) as well as recent (Tél and Gruiz, 2006) books. There are several useful reviews comparing the algorithmic aspects of these measurements and the performance of each fractal dimension: for instance, the *boundary fractal dimension* is treated in Klinkenberg (1994) and Gallant et al. (1994); *self-affine time series analysis* in Malamud and Turcotte (1999) and Pelletier and Turcotte (1999), while the *correlation dimension* was the subject of Kogan's (2007) detailed study. A comparison of computer-simulated examples was given by Behery (2006). The compilation of Sun et al. (2006, Table 1), focusing on the techniques used for the fractal dimension analyses of the surface features extracted by remote sensing, is especially useful for summarizing and comparing the different techniques.

Mandelbrot (2002) proposed to put the most important fractal analysis techniques into a *"toolbox"*, just as the tools of the electricians' and plumbers'. The *"power-law"* figuring in the probability distribution $\Pr\{U > u\} \sim u^{-\alpha}$ describing the distribution of a system's attributes having a size $U > u$ can be used in *Fractal Metrology* as a superior tool for fractal modeling. Levitz (2007) used the notion *"basic toolbox"* to capture forms and patterns, while we applied the term "*toolkit*" as more proper for applied sciences (in Oleschko et al., 2010). For Fractal Metrology we propose to use the original term "toolbox" (or *effective toolbox*), to honor to the pioneering works of Mandelbrot (2002). We shall put inside this box some tools designed by us in addition to the common fractal techniques of one of the available commercial software – *Benoit (1.3)* (SCION Corp., Trusoft, 1999, one of its early versions was reviewed by Seffens, 1999). Each Benoit technique is based on some specific relationship (such as: *power law*) established theoretically, empirically, or by computational experiment between a system attribute and the scale of its observation. The *box-counting* (D_{box}), *perimeter-area* (D_p), *information* (D_i), *mass fractal* (D_m), and *ruler* (D_r) dimensions (and corresponding *Hurst*

exponents) are designed for self-similar sets or curves, while the *rescaled range* (D_{RS}), *power spectrum* (D_{PS}), *roughness/length* (D_r), *variogram* (D_v), and *wavelet* (D_w) dimensions are used for self-affine traces or time series (SCION Corp., Trusoft, 1999). The following discussion will involve only five of the mentioned techniques.

5.3.1 Box dimension (D_B)

The size of a self-similar fractal set has been shown to display a power-law relationship with the measurement scale where the fractal dimension is the exponent of the power-law (Tang and Marangoni, 2006). The *Box Dimension* technique is the classical way to prove the fractal behavior of the studied mathematical, computer-simulated or real physical set and is used in this work to measure the roughness from the space-filling ability of solid and pore networks. In this technique, the counting of boxes containing pixels of the object is accomplished, considering the box as occupied if at least one analyzed intensity value belongs to the box. The following equation is basic for D_{box} calculation:

$$N(d) \sim \frac{1}{d^{D_b}} \qquad (2)$$

where N (counted for a set of box sizes with different orientation) is the number of those boxes of linear size d which contain at least one point of the structure (Fig. 3f).

5.3.2 R/S Analysis ($D_{R/S}$)

The R/S analysis is used to describe the self-similarity properties of time series through the Hurst exponent (Scipioni et al., 2008). This traditional method can be described in terms of the range of partial sums of deviations of values from the mean of a time series, normalized by its standard deviation (Alvarez-Ramirez et al., 2008). The *Rescaled range $R/S(w)$* is defined as (TruSoft, 1999):

$$R/S(w) = \left\langle \frac{R(w)}{S(w)} \right\rangle, \qquad (3)$$

where w is the window length; $R(w)$ is the range of values inside the sampled interval; $S(w)$ is the average standard deviation, angular brackets denote expected values. The following equation shows the power-law relation which can be established between the R/S ratio and window length via the Hurst exponent H:

$$R/S(w) \sim w^H. \tag{4}$$

The linearity of the double logarithmic plot of $R/S(w)$ as a function of w reveals a scaling law, where H is the Hurst exponent which is obtained from the slope of the straight line. The relationship between fractal dimension and Hurst exponent is given by Hardy's (1916) conjecture (see Eq. 1).

5.3.3 Power spectrum (D_{PS})

A powerful method to extract the hidden structural information (such as: periodicities and persistence) from a fluctuating time-series is to calculate its power spectrum (Su and Wu, 2007). The power spectrum method gives a scale invariant measure of fractal dimension since the log-log slope of the power spectrum is invariant to arbitrary rescaling of the input (Wilson, 1997). Usually, the Fast Fourier Transform (FFT) is applied to estimate the power spectrum (Dimri and Prakash, 2001). To obtain an estimate of the fractal dimension, the power spectrum $P(k)$ (where $k=2\pi/\lambda$ is the wavenumber, and λ is the wavelength) is first calculated and plotted on a double logarithmic plot as $P(k)$ versus k. If the time-series is self-affine, this plot should follow a straight line for large wavenumbers, with a negative slope $-b$ which is estimated by regression. The exponent $-b$ is related to the fractal dimension D_{PS} as follows (TruSoft, 1999):

$$D_{PS} = \frac{5-b}{2}. \tag{5}$$

5.3.4 Wavelets (D_W)

Wavelets are localized functions of zero mean, constructed by the linear combination of scaling functions (Bakucz and Krüger-Sehm, 2009). They are especially useful for

Title Page

Abstract | Introduction

Conclusions | References

Tables | Figures

|◄ | ►|

◄ | ►

Back | Close

Full Screen / Esc

Printer-friendly Version

Interactive Discussion

compressing images due to certain wavelet transform properties which are in some ways superior to the conventional Fourier transform (Weisstein, 2010). The Wavelet Method is based on the fact that the wavelet transform of a self-affine trace is also self-affine (Rehman and Siddiqi, 2009). The characteristic measure of wavelet variance analysis is the wavelet exponent, H_w (Malamud and Turcotte, 1999). Wavelets are implemented using trigonometric functions that are oscillating around zero in a non-smooth sweep, and localizing them in the frequency space (Jones and Jelinek, 2001). Consider n wavelet transforms all of them with a different scaling coefficient a_i, let $S_1, S_2, \ldots S_n$ be their standards deviations from zero. Define the ratios $G_1, G_2, \ldots, G_{n-1}$ of the standard deviations as $G_1 = S_1/S_2, G_2 = S_2/S_3, \ldots, G_{n-1} = S_{n-1}/S_n$, and compute the average value of G_i as (TruSoft, 1999):

$$G_{avg} = \frac{\sum_{i=1}^{n-1} G_i}{n-1}. \tag{6}$$

The Hurst exponent (H) is $H = f(G_{avg})$, where f is a heuristic function which describes H by G_{avg} for stochastic self-affine traces (TruSoft, 1999). The mother wavelet in Benoit 1.3 is a step function. Malamud and Turcotte (1999) have underlined that wavelets analysis does not share the power-spectral analysis' inherent problems, such as windowing, detrending etc.

5.4 Measurement uncertainty

We propose to measure the uncertainty in terms of standard deviation (σ). The H and σ values extracted by selected Benoit techniques from the original digital images, firmagrams and PDF were subjected to Person's r and Student's t statistical analyses in order to estimate the statistical significance of the differences between them.

Comparative analysis of the five selected reference measurement tools is realized in the present research following the *Guide to the expression of uncertainty (GUM) in measurement* (2008), published by the Joint Committee for Guides in Metrology

Fractal metrology for biogeosystems analysis

V. Torres-Argüelles et al.

(JCGM). The statement of *measurement uncertainty* is used in its broadest sense as a *doubt* defining it as *a parameter, associated with the result of a measurement, that characterizes the dispersion of the values that could be reasonably attributed to the measurand* (JCGM, 2008, p. 2). The GUM recognizes two types of measurement errors (systematic and random) putting them on a probabilistic basis through the concept of *measurement uncertainty* (JCGM, 2009). The latter is described as *the measure of how well one believes one knows the measurand value* (JCGM, 2009, p. 3).

The *standard uncertainty* is defined as the standard deviation (JCGM, 2008) of the input quantity. We propose to measure the uncertainty of fractal analyses in terms of the standard deviation (σ) for the Benoit results.

The statistical significance of the differences in standard uncertainties of the Benoit's data was quantified by Student's-t and Pearson's r correlation analyses. The Pearson's r correlation matrix (computed by the MINITAB Software, 1998) was constructed as:

$$r_{XY} = \frac{\sum_{i=1}^{n}(X_i - \bar{X})(Y_i - \bar{Y})}{(n-1)S_X S_Y}, \tag{7}$$

where X, Y are all possible pairs of the compared variables, see Tables 7–11. Here, $\bar{X}$ and $\bar{Y}$ are mean values, S_X and S_Y are standard deviations. Student's t-test was carried out for paired variables in the SPSS Inc. (1989–2004) environment.

For the @RISK results we carried out the statistical comparison of the significance of the obtained differences in a few statistics built from the first four moments: mean, variance, kurtosis and skewness (Tables 8–11).

The standard deviations of all used techniques (except the wavelets) were analyzed by the same statistical tests but independently of H. Additionally, the Person's r and Student's t-tests were applied to the three compared soils of contrasting genesis, looking for a correlation between the roughness of their images. Finally, the same two statistical tests were applied to the four statistics yielded by @Risk PDF analysis.

5.5 Measurement function

The rule for *converting a quantity value into the corresponding value of the measurand* is named *a measurement model* (JCGM 200, 2008). We selected the Weierstrass-Mandelbrot function (Berry and Lewis, 1980) as the *measurement model* (JCGM, 2009) which fits well to our experimental data (the *firmagram* as well as the *probability density function*, see later). Developing *a measurement model* corresponds to the *formulation stage of uncertainty evaluation* (JCGM, 2009). The *Weierstrass function* $W_0(t)$ is an everywhere continuous but nowhere differentiable function (NIST, 2010 online Digital Library of Mathematical Functions, DLMF) constituted by the sum of a convergent trigonometric series of the form

$$W_0(t) = \sum_{n=0}^{\infty} \omega^n \exp(2\pi i b^n t), \tag{8}$$

where the subscript in $W_0(t)$ corresponds to "original"; the base b is a real number >1, and the weight ω is written either $\omega = b^{-H}$, with $0 < H < 1$ or as $\omega = b^{D-2}$, where $1 < D = 2 - H < 2$; it can be proven that D is the Minkowski-Bouligand dimension for the graph of $W_0(t)$ (Mandelbrot, 2002, 146–147). Several systems with fractal features (i.e. exhibiting scale invariant roughness) can be described with the modified Weierstrass function introduced by Mandelbrot who added to the series further *subharmonics or quasi-subharmonics*. This special and pathological function, called as Weierstrass-Mandelbrot function (Berry and Lewis, 1980; Wang et al., 2008) is continuous, non differentiable and possesses no scale. It is defined as:

$$W(x) = \sum_{n=-\infty}^{\infty} \frac{(1 - e(i\gamma^n x))e^{i\phi_n}}{\gamma^{(D-2)n}}, (1 < D < 2, \gamma > 1, \phi_n \, arbitrary) \tag{9}$$

where D is the fractal box-dimension of the graph of $W(x)$, γ is a parameter, and the phases ϕ_n can be chosen to make W exhibit deterministic or stochastic behavior.

6 Results and discussion

6.1 Experimental setup

Seventeen micromorphological images of three soils with contrasting structural patterns but with similar clay content and mineralogy (Oleschko, 1981) were used for the statistical comparison of the measurement techniques selected for inclusion in Fractal Metrology. The Chernozem-Solonetz pedological complex was sampled in the same agricultural field (Tambov State, Russia). The undisturbed samples (8 cm×4 cm) were collected with specially designed samplers from the arable horizon of each studied soil. All samples were taken at field moisture in order to conserve the soil's structural pattern. In the laboratory, samples were dried by the acetone replacement method and impregnated with resin. The hardened samples were sectioned horizontally making sure that the natural solid-pore distribution anisotropy derived from the tillage practices is preserved (Fig. 3a, c, e). Thin sections (2 cm×4 cm) with 30 µm thickness, were prepared by standard in Russia petrographic procedure (Parfenova and Yarilova, 1977; Brewer, 1964) and analyzed under the petrographic (Carl Zeiss) microscope. All thin sections and digital images are representative of the structural patterns' original anisotropy.

The Chernozem and Solonetz are located five-ten meters apart of each other, inside the patches of a typical mosaic of a man-induced *Bad Lands* landscape. However, the *Chernozem* is the black soil with the highest known level of sponge-type structure development (Phase 1), while the *Solonetz* is a saline-sodium soil with typical massive pattern and ephemeral fractures derived from the altering expansion/contraction cycles (Phase 2). Solonetz had originated from the Chernozem as a result of chemical degradation due to unsustainable irrigation with saline water. Therefore, the experimental setup was focused to capture the critical behavior and phase transition of the soil's structural pattern during this degradation, applying the above-described Fractal Metrology techniques.

Figures 3a, b, c and 4Aa, Ba, Ca show the representative examples of micromorphological images of Chernozem (Figs. 3a and 4Aa) and Solonetz (Figs. 3c and 4Ba), visualizing their contrasting structural patterns that have resulted in statistically different physical properties (Table 2) and soil behavior. The loss of the original quality is related to the structure's collapse in response to the drastic changes which occurred inside the cation exchange complex where the calcium dominating in Chernozem had been replaced by sodium, resulting in Solonetz formation. The phase transition from the highly connected to massive pattern with water-unstable structure and ephemeral fractures has occurred when the sodium concentration exceeded the permissible (critical) level of the macro- and microaggregates' stability. Because of the universality of phase transitions (Stanley, 1971), we expected the similarity of Hurst exponents in case of both soils regardless of some local details. In our case the divergences of the order parameters at the critical Na content $C_{\mathrm{Na,crit}}$ scale *near* the critical point as $\sim \left| C_{\mathrm{Na,crit}} - C_{\mathrm{Na}} \right|^{-\lambda}$. We tried to capture and visualize this trend for the compared soils, measuring it by Fractal Metrology toolbox. The final comparison was carried out between the structural patterns of both soils and the Chocolate Clay whose massive microstructure had never passed through an aggregation process (Fig. 3e).

The compared images were taken from thin sections using an optical microscope under 10× magnification (Oleschko, 1981).

6.2 Structural patterns comparison

The mean value of the fractal box dimensions for the three compared soils, extracted from the original image and the negative image of the firmagram (Benoit's box counting algorithm is working only on the white part of an image, Fig. 3f) is close to 1.89, the fractal dimension of the Sierpinski carpet (Korvin, 1992), varying between 1.87 (Chernozem) and 1.92 (Solonetz). The data variation is low, with highest mean standard deviation of 0.017 obtained for D_{box} of Chernozem (original image) and the minimal (0.002) for the same soil but when H was extracted from the negative of the firmagram. We concluded that all compared porous materials can be defined as homogeneous

from the point of view of the space filling ability of their solid and pore patterns, and their roughness calculated by the box fractal dimension. Note that the box counting analysis of the firmagram extracts more precise information about the matrix density (solids and pores mutual distribution) inside the original images.

⁵ The apparent independence of the box counting dimension on soil genesis for the studied pedological complex compared with Chocolate Clay (porous material which can not be named soil) can be observed in Table 1. This independence can be interpreted as empirical evidence for some generic features (universality?) of roughness of these materials with similar clay mineralogy (micro-scale) but contrasting appearance ¹⁰ of structural patterns (macro-scale). Therefore, neither the box fractal dimension nor the standard deviation were able to detect any differences in the roughness of digital images of the compared soils.

Our previous physical experiments, and corresponding computer simulations, have shown similar trends for soils of different genesis (Oleschko et al., 2000). Fractal analy- ¹⁵ sis of multiscale soil images, firmagrams as well as observed and computer-simulated microwaves scattered from soil (has not been done in the present study), yielded simi- lar values for the fractal parameters (Oleschko et al., 2002, 2003).

In Table 2 the microaggregate composition of the Chernozem and Solonetz esti- mated by the reference pipette method (Vadyunina and Korchagina, 1973) are com- ²⁰ pared for two genetic horizons. The high content of physical clay (the physically active fraction of particles with size <0.01 mm, considered as most important for microag- gregation) in both soils ensures their suitability to form clusters of fine particles (mi- croaggregates). Notwithstanding, the differences in the nature of the dominant cation in CEC are responsible for contrasting physical and chemical properties of Chernozem ²⁵ and Solonetz. We speculate that the similarity in roughness between these soils is due to their high physical clay content, which increased significantly with depth (Oleschko, 1980).

The Person's *r* analysis as well as the Student *t*-test show the strongly significant correlations between the roughness of all compared soils and therefore non significant

Full Screen / Esc

Printer-friendly Version

Interactive Discussion

differences, independently on the applied measurement techniques (Tables 3 and 4).

6.3 Uncertainty of fractal measurements

As the second step of measurements protocol, the Hurst exponent values, extracted from the images, firmagrams and PDFs by Box Counting, Rescaled-Range, Power Spectrum and Wavelets techniques were compared as regards the mean value of the Hurst exponent and its standard deviation (Table 5). The H_{RS} extracted from the original images transformed into time series (ts) has highest mean value in Chernozem (0.064) as compared with Solonetz (0.039) and Clay (0.031). The mean standard deviation shows the same tendency: its value is higher for the H_{RS} of Chernozem (0.742) in comparison with Solonetz (0.362) and Chocolate Clay (0.377). We note that the Chernozem's standard deviation measured by Rescaled Range technique (0.742) is more than almost 50 times larger than for Box Counting (0.017).

As in the case of box counting (Table 5), the standard deviation was smaller for H_{RS} extracted from the firmagrams, being equal to 0.193 for Chernozem and minimal for Clay (0.104). The mean value of H_{RS} measured for the firmagrams three soils was 0.229, and therefore the corresponding mean fractal dimension was $D_{RS}=1.771$. The values of roughness measured by the power spectrum method applied on the original images and firmagrams were comparable with those values obtained by the R/S technique (except the "Clay" samples where the fractal dimension has reached the topological limit of 2): the mean value of H_{PS} is equal to 0.208 for images. For all techniques the roughness information extracted from the PDF was noisier in comparison with the two other sources namely original digital images and firmagrams. In spite of the listed differences between the differently measured Hurst exponents, these were not statistically significant only for four compared standard deviation pairs (Tables 5 and 6). The H values measured by Wavelets technique fluctuated around 0.5 (the Hurst exponent value of white noise) similarly to the above-discussed PDF case. We concluded that the Wavelets technique was not sufficiently precise for the roughness measurement of the compared soils.

The mean H_{RS} value measured on the firmagram was equal to 0.229 (with standard deviation 0.141) showing that the H_{RS} extracted from the original image has higher roughness (mean H_{RS}=0.044) and higher uncertainty (S_{RS}=0.493). The power spectrum technique gave the similar mean H_{PS} value of 0.208 for the original images of the compared soils, showing higher roughness for the firmagram (H_{PS}=0.048). The values of H_w measured by Wavelets method fluctuated around 0.5 for images, firmagrams and PDF, the mean H_w value was equal to 0.40 for the original images (Table 5).

This conclusion is confirmed by Pearson's r analysis where 45 different pairs of H were compared (Table 7), showing the statistically significant correlation at the 0.01 level among 7 of them, at the level 0.05 among four pairs, and uncorrelated values of the remaining 34 pairs. However, it is notable that among these 34 pairs, 23 correspond to the Hurst exponents measured by wavelets technique (which have correlated negatively −0.80, and only once with the H_{RS} of soil firmagrams) while the other eleven have correlation coefficients close to 0.45.

In spite of the statistical similarity between the compared soils' roughness (Table 4), the *precision* of the compared techniques measured in terms of standard deviation was significantly different, except for the following pairs which show significant correlation: $S_{box(image)}$ versus $S_{box(firmagram)}$ with correlation coefficient of −0.528; $S_{RS(image)}$ and $S_{PS}(image)$, where r=−0.72, (Table 6).

The outlier (high) standard deviation values of the spectral dimension might be due to the special construction of the time series extracted from the digital images and firmagrams. In the image one should expect a spatial correlation over a distance of a few pixel-sizes between the neighboring values $p_{i,j}; p_{i\pm1,j}; p_{i\pm2,j}; \dots$. Because of this, some artificial periodicity in the firmagram of period $\approx N$ could have appeared, so that the lags, window-length, etc., used to estimate H or D from the images and firmagrams must be kept much less than image size N in order to avoid this artifact.

Statistical comparison was also accomplished among the central moments (mean, variance, kurtosis, skewness) of the empirical and theoretical PDFs extracted by the @Risk software, confirming the similarity of the gray-level distribution across the

Chernozem-Solonetz pedological complex images and the Chocolate Clay (Tables 8–11). We speculate that the influence of microstructure and soil mineralogy on image roughness is more important than all other attributes characteristic for the macrofeatures of the structural pattern. The detailed architecture of Solonetz on the microscale

5 preserved the original Chernozem features, conserving the self-organizing capacity of the fine matrix near the transition point when sodium content overpasses the critical value. This catastrophic event, known as *soil chemical degradation*, involves a *structural phase transition* detectable by visual comparison of microscopic images. The Chernozem aggregates collapsed at all hierarchical levels, resulting in the massive

10 pattern of Solonetz, where the major attraction between the solid particles (with high content of montmorillonites) is responsible for the low inter-aggregate porosity and high fracture density. This re-arrangement of structural patterns does not cause statistically significant changes in the scale-invariance of the microstructure. However, in spite of the statistically insignificant differences of the Hurst exponent values, the *H* values of

15 Solonetz and Chocolate Clay for some techniques tend to be smaller, indicating higher roughness (Table 5). These changes can be interpreted as indications of the breakdown of interconnected porosity in Solonetz, due to the soil's chemical degradation. In most of the analyzed cases the roughness of the micromorphological images has antipersistent character.

20 **7   Conclusions**

The presented results of applying the *Fractal Metrology toolbox* to three soils with contrasting structural patterns but very similar mineralogy prove the effectiveness of certain fractal descriptors for measuring the dynamics of complex systems. The box counting dimension extracted from the images and *firmagrams* was more precise in

25 terms of standard deviation in comparison with the three other techniques selected for testing. The Rescaled-Range method extracted similar values for the digital images' roughness, but its uncertainty was several times higher. The power spectrum technique

Fractal metrology for biogeosystems analysis

V. Torres-Argüelles et al.

Title Page

Abstract | Introduction

Conclusions | References

Tables | Figures

|◄ | ►|

◄ | ►

Back | Close

Full Screen / Esc

Printer-friendly Version

Interactive Discussion

yields results close to those in case of the box- and R/S analyses but it has incomparably higher uncertainty probably due to the artificial construction of the *firmagrams*. The wavelets technique was not able to extract meaningful roughness estimates from the studied images, the resulting H values fluctuated around $H=0.5$ characteristic for white noise. Similar tendency was found for the Hurst values extracted from the PDFs of gray intensities. Notwithstanding, the statistically significant similarity between the roughness of Chernozem and Solonetz belonging to the same pedological complex affected by salinization proves the suitability of the proposed step by step technique to look for the critical behavior of soil structural patterns related with degradation. The selected toolbox can be useful for the quantification of the spatio-temporal dynamics and behavior of other Earth systems, especially in similar cases of phase-transition. We conclude that a combined use of different fractal descriptors ensures the required statistical control for fractal measurements of complex system attributes and behavior, and provides data for unbiased comparison. The optimal selection of fractal parameters to capture critical behavior and phase transition should be tested for each specific application.

References

Alvarez-Ramirez, J., Echeverria, J. C., and Rodriguez, E.: Performance of a high-dimensional R/S method for Hurst exponent estimation, Physica A, 387, 6452–6462, 2008.

Bakucz, P. and Krüger-Sehm, R.: A new wavelet filtering for analysis of fractal engineering surfaces, Wear, 266, 539–542, 2009.

Barton, C. C. and La Pointe, P. R.: Fractals in Petroleum Geology and Earth Processes, Springer, New York, 1995.

Bassler, K. E., Gunaratne, G. H., and McCauley, J. L.: Markov processes, Hurst exponents, and nonlinear diffusion equations: with application to finance, Physica A, 369, 343–353, 2006.

Behery, G. M.: Simulation of fractal dimension evaluations, Int. J. Model. Simul., 26, 91–97, 2006.

5 Beiró, M. G., Alvarez-Hamelin, J. I., and Busch, J. R.: A low complexity visualization tool that helps to perform complex systems analysis, New, J. Phys., 10, 125003, doi:10.1088/1367-2630/10/12/125003, 2008.

Berry, M. V.: Quantum fractals in boxes, J. Phys. A-Math. Gen., 29, 6617–6629, 2006.

Berry, M.: Why are special functions special?, Phys. Today, 54, 11–12, 2001.

10 Berry, M. V. and Lewis, Z. V.: On the Weierstrass-Mandelbrot fractal function, Proc. R. Soc. Lon. Ser. A, 370, 459–484, 1980.

Bigerelle, M., Gautier, A., and Iost, A.: Roughness characteristic length scales of micro-machined surfaces: a multi-scale modeling, Sensor. Actuat. A-Phys., 126, 126–137, 2007.

Borri-Brunetto, M., Carpinteri, A., and Chiaia, B.: Scaling phenomena due to fractal contact in
15 concrete and rock fractures, Int. J. Fracture, 95, 221–238, 1999.

Brink, L.: The Nobel Prize in Physics 2008, Presentation Speech, http://nobelprize.org/nobel_prizes/physics/laureates/2008/presentation-speech.html, last access: 15 June 2010, 2008.

Chandrasekaran, S. and Sundararajan, S.: Effect of microfabrication processes on surface roughness parameters of silicon surfaces, Surf. Coat. Tech., 188–189, 581–587, 2004.

20 Chang, K. J., Ray, G., Bradbury, D., Nakagawa, O. S., Oh, S.-Y., Bartelink, D., Chang, E., Stine, B., Maung, T., Divecha, R., Boning, D., and Chung, J.: Using a statistical metrology framework to identify systematic and random sources of die- and wafer-level ILD thickness variation in CMP processes, IEDM Tech. Digest, 499–502, Dec. 1995.

Christensen, K. and Moloney, N. R.: Complexity and Criticality, Imperial College Press Ad-
25 vanced Physics Texts, vol. 1, Imperial College Press, London, 2005.

Cox, M. G., Rossi, G. B., Harris, P. M., and Forbes, A.: A probabilistic approach to the analysis of measurement processes, Metrologia, 45, 493–502, 2008.

Cox, S.: Information technology: the global key to precision agriculture and sustainability, Comput. Electron. Agr., 36, 93–111, 2002.

30 Curtis, M. and Farago, F.: Handbook of Dimensional Measurement, fourth edn., Industrial Press Inc., New York, USA, 2007.

Denisov, S. I.: Fractal dimension of random processes, Chaos Soliton. Fract., 9, 1491–1496, 1998.

Fractal metrology for biogeosystems analysis

V. Torres-Argüelles et al.

Title Page

Abstract	Introduction
Conclusions	References
Tables	Figures

◄◄   ►►

◄   ►

Back   Close

Full Screen / Esc

Printer-friendly Version

Interactive Discussion

Diehl, R. J. and Holm, P.: Roughness measurements – have the necessities changed?, J. Sound Vib., 293, 777–783, 2006.

Dimri, V. P. and Prakash, M. R.: Scaling of power spectrum of extinction events in the fossil record, Earth Planet. Sc. Lett., 186, 363–370, 2001.

Dodds, P. S.: Optimal form of branching supply and collection networks, Phys. Rev. Lett., 104, 048702, doi:10.1103/PhysRevLett.104.048702, 2010.

Eberhardt, K., Hagwood, C., Kacker, R., Levenson, M., Liu, H. K., Vangel, M., Yen, J., and Zhang, N. F.: 5.6 Bayesian Metrology, in: Report of activities of the statistical engineering division, edited by: US Department of Commerce, Technology Administration, NIST, http://www.itl.nist.gov/div898/pubs/ar/ar2000/node40.html, last access: 15 June 2010, 2000.

Ellis, C.: The sampling properties of Hurst exponent estimates, Physica A, 375, 159–173, 2007.

El-Sonbaty, I. A., Khashaba, U. A., Selmy, A. I., and Ali, A. I.: Prediction of surface roughness profiles for milled surfaces using an artificial neural network and fractal geometry approach, J. Mater. Process. Technol., 200, 271–278, 2008.

Falconer, K.: Techniques in Fractal Geometry, John Wiley & Sons, 274 pp., Chicester – New York – Brisbane – Toronto – Singapure, 1997.

Feagin, R. A.: Relationship of second order lacunarity, Brownian motion, Hurst exponent, and pattern organization, Physica A, 328, 315–321, 2003.

Feagin, R. A., Wu, X. B., and Feagin, T.: Edge effects in lacunarity analysis, Ecol. Modell., 201, 262–268, 2007.

Finch, S. R.: E: Unusual numbers, http://listserv.nodak.edu/scripts/wa.exe?A2=ind0108&L=NMBRTHRY&F=&S=&P=963, last access: 27 August 2001.

Finch, S. R.: Stieltjes Constants, Mathematical Constants, Cambridge University Press, Cambridge, UK, 166–171, 2003.

Fleming, R. W., Dror, R. O., and Adelson, E. H.: Real-world illumination and the perception of surface reflectance properties, J. Vision, 3, 347–368, 2003.

Fransson, J. H. M., Talamelli, A., Brandt, L., and Cusso, C.: Delaying transition to turbulence by a passive mechanism, Phys. Rev. Lett., 96, 6, doi:10.1103/PhysRevLett.96.064501, 2006.

Gallant, J. C., Moore, I. D., and Hutchinson, M. F.: Estimating fractal dimension of profiles: a comparison of methods, Math. Geol., 26, 455–481, 1994.

Germer, T. A.: Measurement of roughness of two interfaces of a dielectric film by scattering ellipsometry, Phys. Rev. Lett., 85, 349–352, 2000.

Title Page

Abstract	Introduction
Conclusions	References
Tables	Figures

◄	►
◄	►
Back	Close

Full Screen / Esc

Printer-friendly Version

Interactive Discussion

Discussion Paper | Discussion Paper | Discussion Paper | Discussion Paper | Discussion Paper

Gomez, S., Hale, K., Burrows, J., and Griffiths, B.: Measurements of surface defects on optical components, Meas. Sci. Technol., 9, 607–616, 1998.

Grimm, V., Revilla, E., Berger, U., Jeltsch, F., Mooij, W. M., Railsback, S. F., Thulke, H.-H., Weiner, J., Wiegand, T., and DeAngelis, D. L.: Pattern-oriented modeling of agent-based complex systems: lessons from ecology, Science, 310, 987–991, 2005.

Hardy, G. H.: A Mathematician's Apology, 1940, avalaible at: http://www.math.ualberta.ca/mss/, last access: 15 June 2010, 2005.

Hardy, G. H.: Weierstrass's non-diferentiable function, T. Am. Math. Soc., 17, 301–325, 1916.

Heilmann, R. K., Chen, C. G., Konkola, P. T., and Schattenburg, M. L.: Dimensional metrology for nanometer-scale science and engineering, IEEE Conference on Nanoscale Devices system Integration, Miami FL, 15–19 Feb 2004, Nanotechnology (preprinted), 2004.

Hopp, T. H.: Computational metrology, Manuf. Rev. (American Society of Mechanical Engineers, New York), 6, 295–304, 1993.

Hurst, H. E.: Long-term storage capacity of reservoirs, Trans. Am. Soc. Civ. Eng., 116, 770–808, 1951.

International Organization for Standarization (ISO): International Vocabulary of Basic and General Terms in Metrology, 3rd edn., Geneva, Switzerland, 2004.

Jensen, J. E.: Computationally modeling the effects of surface roughness on soft X-ray multi-layer reflectors, M.S. thesis, Department of Physics and Astronomy, Brigham Young University, Provo, Utah, USA, 164 pp., 2006.

Joint Committee for Guides in Metrology (JCGM): International Vocabulary of Metrology – Basic and General Concepts and Associated Terms, 3rd edn., Geneva, Switzerland, 2008.

Joint Committee for Guides in Metrology (JCGM): Evaluation of Measurement Data – An Introduction to the "Guide to the Expression of Uncertainty in Measurement" and Related Documents, first edn., Geneva, Switzerland, 2009.

Jones, C. L. and Jelinek, H. F.: Wavelet packet fractal analysis of neuronal morphology, Methods, 24, 347–358, 2001.

Kaneko, K.: Clustering, coding, switching, hierarchical ordering, and control in a network of chaotic elements, Physica D, 41(9), 137–172, 1990.

Katz, J. S.: Indicators for complex innovation systems, Res. Policy, 35, 893–909, 2006.

Kim, T. W., Bhushan, B., and Cho, Y. J.: The contact behavior of elastic/plastic non-Gaussian rough surfaces, Tribol. Lett., 22, 1–13, 2006.

Klinkenberg, B.: A review of methods used to determine the fractal dimension of linear features,

Title Page

Abstract | Introduction

Conclusions | References

Tables | Figures

◀ | ▶

◀ | ▶

Back | Close

Full Screen / Esc

Printer-friendly Version

Interactive Discussion

Math. Geol., 26, 23–46, 1994.

Korvin, G.: Fractal Models in the Earth Sciences, Elsevier, Amsterdam, 396 pp., 1992.

Korvin, G.: Is the optical image of a non-Lambertian fractal surface fractal?, IEEE Geosci. Remote S., 2, 380–383, 2005.

Levitz, P.: Toolbox for 3-D imaging and modeling of porous media: relationship with transport properties, Cement Concrete Res., 37, 351–359, 2007.

Lojkowski, W., Turan, R., Proykova, A., and Daniszewska, A. (Eds.): Eighth nanoforum report: nanometrology, http://www.co-nanomet.eu/content/Co-nanomet%20protected%20documents/training%20and%20resources/library/Eighth%20Nanoforum%20Report_%20Nanometrology.pdf, last access: 15 June 2010, 2006.

Lu, X. and Guan, J.: A new approach to building histogram for selectivity estimation in query processing optimization, Comput. Math. Appl., 57, 1037–1047, 2009.

Majumdar, A. and Bhushan, B.: Fractal model of elastic-plastic contact between rough surfaces, ASME J. Tribol., 113, 1–11, 1991.

Malamud, B. D. and Turcote, D. L.: Self-affine time series: measures of weak and strong persistence, J. Stat. Plan. Infer., 80, 173–196, 1999.

Mandelbrot, B. B.: The Fractal Geometry of Nature, W. H. Freeman and Company, New York, USA, 1982.

Mandelbrot, B. B.: Gaussian Self-Affinity and Fractals, Springer-Verlag, New York, 2002.

Mandelbrot, B. B. and Van Ness, J. W.: Fractional Brownian motions, fractional noises and applications, SIAM Rev., 10, 422–437, 1968.

Mandelbrot, B. B. and Wallis, J. R.: Noah, Joseph and operational hydrology, Water Resour. Res., 4, 909–918, 1968.

Mandelbrot, B. B., Passoja, D. E., and Paulay, A. J.: Fractal character of fracture surfaces of metals, Nature, 308, 721–722, 1984.

Marschal, A., Andrieux, T., Compagon, P. A., and Fabre, H.: Chemical metrology – QUID?, Accredit. Qual. Assur., 7, 42–49, 2002.

MINITAB for Windows: MAVV. Home. WIN 1221.03737, http://www.minitab.com, last access: 15 June 2010, 1998.

Monroe, D.: Rough skin is good, Phys. Rev. Focus, http://focus.aps.org/story/v17/st6, last access: 15 June 2010, 17 Feb 2006.

Monroe, D.: Why leaves aren't trees, Phys. Rev. Focus, http://focus.aps.org/story/v25/st4, 4 Feb 2010.

Title Page

Abstract | Introduction

Conclusions | References

Tables | Figures

|◄ | ►|

◄ | ►

Back | Close

Full Screen / Esc

Printer-friendly Version

Interactive Discussion

Nambu, Y.: Nobel lecture: spontaneous symmetry breaking in particle physics: a case of cross fertilization, presented by: Jona-Lasinio, G., http://nobelprize.org/nobel_prizes/physics/laureates/2008/nambu-lecture.html, last access: 15 June 2010, 2008.

NIST: Bayesian metrology, National Institute of Standards and Technology, Manufacturing Engineering Laboratory, 2001.

NIST/SEMATECH: e-Handbook of statistical methods, Probability density function, http://www.itl.nist.gov/div898/pubs/ar/ar1999/node46.html,, Gaithersburg, MD, USA, 2006.

National Institute of Standards and Technology (NIST): Digital library of mathematical functions, http://dlmf.nist.gov/, 2010.

Oleshko, K., Vadiunina, A. F., Zilaeva, V. A., and Truchin, V. I.: Influencia del campo magnético sobre las propiedades del suelo y plantas (in russian), Pochvovedenie, 7, 91–100, 1980.

Oleschko, K.: Effect of electric current on clay minerals in "chocolate" clays, Universidad Estatal de Moscú M. V. Lomonósov, Facultad de Suelos (en ruso), Boletín de la Universidad de Moscú, serie Pochvovedenie, Edafología, 2, 1981.

Oleschko, K., Figueroa, B., Miranda, M. E., Vuelvas, M. A., and Solleiro, R. E.: Mass fractal dimensions and some selected physical properties of contrasting soils and sediments of México, Soil Till. Res., 55, 43–61, 2000.

Oleschko, K., Korvin, G., Balankin, A. S., Khachaturov, R. V., Flores, Figueroa, L., Urrutia, J., and Brambila, F.: Fractal scattering of microwaves from soils, Phys. Rev. Lett., 89, 188501, doi:10.1103/PhysRevLett.89.188501, 2002.

Oleschko, K., Korvin, G., Figueroa, B., Vuelvas, M. A., Balankin, A., Flores, L., and Carreon, D.: Fractal radar scattering from soil, Phys. Rev. E, 67, 041403–1:041403–13, 2003.

Oleschko, K., Figueroa-Sandoval, B., Korvin, G., and Martínez-Menes, M.: Agroecometría: una caja de herramientas para el diseño de una agricultura virtual, Agricultura, Sociedad y Desarrollo, 1, 53–71, 2004.

Oleschko, K., Parrot, J.-F., Korvin, G., Esteves, M., Vauclim, M., Torres-Argüelles, V., Gaona-Salado, C., and Cherkasov, S.: Fractal image informatics: from SEM to DEM, Proceedings of 4th International Conference: GIS in Geology and Geosciences, Vista of New Approaches for the Geoinformatics, AIP Conf. Proc., 109, 2509–2517, 2008.

Oleschko, K., Korvin, G., Flores, L., Brambila, F., Gaona, C., Parrot, J.-F., Ronquillo, G., and Zamora, S.: Probability density function: a tool for simultaneous monitoring of pore/solid roughness and moisture content, Geoderma, available at: http://www.sciencedirect.com/science?_ob=ArticleURL&_udi=B6V67-4XRBH4D-2&_user=945819&_coverDate=

Fractal metrology for biogeosystems analysis

V. Torres-Argüelles et al.

Title Page

Abstract	Introduction
Conclusions	References
Tables	Figures

|◄ | ►|
◄ | ►

Back | Close

Full Screen / Esc

Printer-friendly Version

Interactive Discussion

11%2F19%2F2009&_rdoc=1&_fmt=high&_orig=search&_sort=d&_docanchor=&view= c&_searchStrId=1346583153&_rerunOrigin=google&_acct=C000048981&_version= 1&_urlVersion=0&_userid=945819&md5=e40b1edc361036214c3107019c2a69c5, 2010.

Orbach, R.: Dynamics of fractal networks, Science, 231, 814–819, 1986.

Palisade Corporation: Guide to Using @RISK: Risk Analysis and Simulation Add-In for Microsoft® Excel Version 5.5, 2005.

Pafenova, E. I. and Yarilova, E. A.: Guide on micromorphological studies in soil science, Nauka, Moscow, 198 pp, 1977.

Parrot, J. F.: Hist-Gen General algorithm for histogram, Universidad Nacional Autónoma de México (in Spanish, unpublished), 2003.

Partis, L., Croan, D., King, B., and Emslie, K. R.: Biometrology and biomeasurement: overview of current technologies and priorities for a biological measurement program in Australia, Australian Government Analytical Laboratories, Pymble, NSW, Australia, AGAL Public Interest Program Public, Interest Report Series Number, 2002-1, 2002.

Paschotta, R.: Encyclopedia of Laser Physics and Technology, RP Photonics, Zürich, Switzerland, 2009.

Pawley, J. B.: Handbook of Biological Confocal Microscopy, 3rd edn., Springer Science + Business media, New York, 985 pp., 2006.

Pelletier, J. D. and Turcotte, D. L.: Self-affine time series: 11. Applications and models, Adv. Geophys., 40, 91–166, 1999.

Pendleton, D. E., Dathe, A., and Baveye, P.: Influence of image resolution and evaluation algorithm on estimates of the lacunarity of porous media, Phys. Rev. E, 72, 041306, doi:10.1103/PhysRevE.72.041306, 2005.

Pentland, A. P.: Fractal based description of natural scenes, IEEE T. Pattern Anal., PAMI-6, 661–674, 1984.

Plowman, D. A., Solansky, S., Beck, T. E., Baker, L., Kulkarni, M., and Villarreal Travis, D.: The role of leadership in emergent, self-organization, Leadership Quart., 18, 341–356, 2007.

Puente, C.: A universe of projections: may Plato be right?, Chaos Soliton. Fract., 19, 241–253, 2004.

Rehman, S. and Siddiqi, A. H.: Wavelet based hurst exponent and fractal dimensional analysis of Saudi climatic dynamics, Chaos Soliton. Fract., 40, 1081–1090, 2009.

Rodriguez-Iturbe, I. and Rinaldo, A.: Fractal River Basins: Chance and Self-Organization, Cambridge University Press, New York, 564 pp., 1997.

Fractal metrology for biogeosystems analysis

V. Torres-Argüelles et al.

Title Page

Abstract	Introduction
Conclusions	References
Tables	Figures

|◄| |►||

|◄| |►|

Back | Close

Full Screen / Esc

Printer-friendly Version

Interactive Discussion

SCION Corp.: BENOIT 1.3, http://www.scioncorp.com, 1999.

Scipioni, A., Rischette, P., Bonhomme, G., and Devynck, P.: Characterization of self-similarity properties of turbulence in magnetized plasmas, Phys. Plasmas, 15, 112303, doi:10.1063/1.3006075, 2008.

Seffens, W.: Order from chaos, techsighting software, Science, 285, 5431, doi:10.1126/science.285.5431.1228a, 1999.

SFL: Surface Metrology Laboratory (SML), Surface Metrology, Departament of Mechanical Engineering, Worcester Polytechnic Institute, http://www.me.wpi.edu/Research/SurfMet/, last access: 15 June 2010, 2008.

Stanley, H. E.: Introduction to Phase Transitions and Critical Phenomena, Oxford University Press, 336 pp., New York, USA, 1971.

Statistical Package for the Social Sciences (SPSS): 13.0 for Windows, Copyright© SPSS Inc., 1989–2004.

Strauss, O.: Quasi-continuous histograms, Fuzzy Set. Syst., 160, 2442–2465, 2009.

Su, Z.-Y., and Wu, T.: Music walk, fractal geometry in music, Physica A, 380, 418–428, 2007.

Sun, W., Xu, G., Gong, P., and Liang, S.: Fractal analysis of remotely sensed images: a review of methods and applications, Int. J. Remote Sens., 27, 4963–4990, 2006.

Tancrez, J.-S., Semal, P., and Chevalier, P.: Histogram based bounds and approximations for production lines, Eur. J. Oper. Res., 197, 1133–1141, 2009.

Tang, D. and Marangoni, A. G.: 3-D fractal dimension of fat crystal networks, Chem. Phys. Lett., 433, 248–252, 2006.

Tél, T. and Gruiz, M.: Chaotic Dynamics: An Introduction Based on Classical Mechanics, Cambridge University Press, 393 pp., Cambridge, UK, 2006.

TruSoft, Intern. Inc.: Benoit 1.3 Software, 1999.

Turcotte, D. L.: Fractals and Chaos in Geology and Geophysics, Cambridge University Press, 416 pp., Cambridge, UK, 1997.

Vadyunina, A. F. and Korchagina, Z. A.: Methods of Studies of Physical Properties of Soils, Academy School Publishers, (in Russian), 416 pp., 1973.

Vadyunina, A. F., Sokolova, T. A., Oleshko, K., and El Lakani, A. A.: Effect of electric current on clay minerals in "Chocolate Clays", Vestnik MGU (Pochvovedenie, in Russian), Moscow, 50–54, 1980.

Van Gorp, A., Bigerelle, M., Grellier, A., Iost, A., and Najjar, D.: A multi-scale approach of roughness measurements: evaluation of the relevant scale, Mat. Sci. and Eng. C, 27, 1434–

1438, 2007.

Verhoest, N. E. C., Lievens, H., Wagner, W., Álvarez-Mozos, J., Moran, M. S., and Mattia, F.: On the soil roughness parameterization problem in soil moisture retrieval of bare surfaces from synthetic aperture radar (Review), Sensors, 8, 4213–4248, 2008.

5   Villarrubia, J. S.: Issues in line edge and line width roughness metrology, AIP Conference proceedings: Characterization and metrology for ULSI Technology, 386–393, 2005.

Wang, L., Rong, W., and Sun, L.: Elastic-plastic adhesive contact of fractal microparts surfaces with low adhesion parameters, Proceedings of the 3rd IEEE Int. Conf. on Nano/Micro Engineered and Molecular Systems, Sanya, China, 6–9 Jan, 592–595, 2008.

10   Weisstein, E. W.: From MathWorld – a Wolfram web resource, http://mathworld.wolfram.com/, 2010.

Willink, R.: Principles of probability and statistics for metrology, Metrologia, 43, S211–S219, 2005.

Wilson, T. H.: Short notice, Fractal strain distribution and its implications for cross-section balancing: further discussion, J. Struct. Geol., 19, 129–132, 1997.

Title Page

Abstract   Introduction

Conclusions   References

Tables   Figures

◄   ►

◄   ►

Back   Close

Full Screen / Esc

Printer-friendly Version

Interactive Discussion

Table 1. Hurst exponent (H), fractal dimension (D) and standard deviation (S) measured by box counting method for seventeen analyzed images of three soils and their respective firmagrams.

Image	D_{box}			D_{box} firmagram		
	H	D	S	H	D	S
D-13-Chernozem	0.083	1.917	0.017	0.075	1.925	0.002
D-19-Chernozem	0.083	1.917	0.016	0.23	1.77	0.001
D-1-Solonetz	0.116	1.884	0.018	0.127	1.873	0.001
D-2- Solonetz	0.09	1.91	0.008	0.119	1.881	0.01
D-3- Solonetz	0.102	1.898	0.014	0.129	1.871	0.005
D-14- Solonetz	0.107	1.893	0.015	0.092	1.908	0.006
D-16- Solonetz	0.103	1.897	0.015	0.109	1.891	0.002
D-17- Solonetz	0.104	1.896	0.014	0.124	1.876	0.008
D-18- Solonetz	0.083	1.917	0.015	0.13	1.87	0.008
D-4-Clay	0.134	1.866	0.024	0.139	1.861	0.001
D-5-Clay	0.109	1.891	0.01	0.111	1.889	0.001
D-6-Clay	0.133	1.867	0.011	0.087	1.913	0.008
D-7-Clay	0.101	1.899	0.006	0.085	1.915	0.009
D-9-Clay	0.094	1.906	0.01	0.156	1.844	0.002
D-10-Clay	0.116	1.884	0.012	0.069	1.931	0.004
D-11-Clay	0.126	1.874	0.014	0.124	1.876	0.001
D-12-Clay	0.124	1.876	0.018	0.077	1.923	0.004
Mean	0.106	1.894	0.014	0.117	1.883	0.004
Maximum	0.134	1.917	0.024	0.230	1.931	0.010
Minimum	0.083	1.866	0.006	0.069	1.770	0.001
S	0.017	0.017	0.004	0.038	0.038	0.003

Full Screen / Esc

Printer-friendly Version

Interactive Discussion

Table 2. The microaggregate composition of the Chernozem and Solonetz soils at different depths.

Soil	Depth (cm)	Microaggregate fraction (%)						
		1–0.25 (%)	0.05–0.01	0.01–0.005	0.005–0.001	<0.001	<0.01	>0.01
Chernozem	(0–20)	0.0	46.9	17.8	8.2	2.5	28.5	71.5
	(40–50)	0.2	44.8	15.8	17.7	2.7	36.2	63.8
Solonetz	(0–20)	0.0	46.5	21.5	13.5	9.9	44.9	55.1
	(40–50)	0.0	21.1	17.6	12.3	45	74.9	25.1

Title Page

Abstract | Introduction

Conclusions | References

Tables | Figures

◀◀ | ▶▶

◀ | ▶

Back | Close

Full Screen / Esc

Printer-friendly Version

Interactive Discussion

Table 3. Pearson's *r* correlation matrix for the Hurst exponent of three studied soils.

	Clay	Solonetz	Chernozem
Clay	1	0.872[**] 0.001	0.909[**] 0
Solonetz		1	0.870[**] 0.001
Chernozem			1

[*] Correlation is significant at the 0.05 level (2-tailed).
[**] Correlation is significant at the 0.01 level (2-tailed).

Table 4. Student t-test for the Hurst exponents of three compared soils.

	Paired differences						t	df	Sig. (2-tailed)
	Mean	S	SEM	95% confidence interval of the difference					
				Lower	Upper				
Clay - Solonetz	0.025	0.101	0.032	−0.047	0.097		0.786	9	0.452
Clay - Chernozem	0.021	0.086	0.027	−0.041	0.083		0.771	9	0.461
Solonetz - Chernozem	−0.004	0.087	0.028	−0.066	0.058		−0.146	9	0.887

[*] The differences are significant at the 0.05 level (2-tailed).
[**] The differences are significant at the 0.01 level (2-tailed).

Table 5. Hurst exponent (H) and standard deviation (S) for each soil type and technique used.

	Total mean	Chernozem	Solonetz	Clay
$H_{box(image)}/S_{box(image)}$	0.100/0.014	0.083/0.017	0.101/0.014	0.117/0.013
$H_{box(firmagram)}/S_{box(firmagram)}$	0.125/0.004	0.153/0.002	0.119/0.006	0.106/0.004
$H_{RS(image)}/S_{RS(image)}$	0.044/0.493	0.064/0.742	0.039/0.362	0.031/0.377
$H_{RS(PDF)}/S_{RS(PDF)}$	0.444/0.007	0.424/0.006	0.505/0.010	0.404/0.006
$H_{RS(firmagram)}/S_{RS(firmagram)}$	0.229/0.141	0.270/0.193	0.201/0.127	0.217/0.104
$H_{PS(image)}/S_{PS(image)}$	0.208/144 302.145	0.151/133 766.650	0.233/146 878.879	0.241/152 260.906
$H_{PS(PDF)}/S_{PS(PDF)}$	0.417/11.244	0.454/10.960	0.435/14.941	0.366/7.831
$H_{PS(firmagram)}/S_{PS(firmagram)}$	0.048/40 068.195	0.121/48 708.625	0.024/38 070.717	0.000/33 425.244
$H_{W(image)}$	0.400	0.413	0.360	0.428
$H_{W(PDF)}$	0.560	0.565	0.426	0.689
$H_{W(firmagram)}$	0.427	0.319	0.466	0.497

Table 6. Pearson's r correlation matrix for the standard deviations (S) of three applied techniques: Box dimension, R/S analysis and Power spectrum.

	S_{box} (image)	S_{box} (firmagram)	S_{RS} (image)	S_{RS} (PDF)	S_{PS} (image)	S_{PS} (PDF)
$S_{box(image)}$	1	−0.528* 0.029	0.059 0.821	−0.013 0.960	−0.207 0.426	0.179 0.492
$S_{box(firmagram)}$		1	−0.249 0.336	0.286 0.266	−0.128 0.625	0.126 0.629
$S_{RS(image)}$			1	0.014 0.959	−0.715** 0.001	−0.321 0.210
$S_{RS(PDF)}$				1	−0.012 0.965	0.475 0.054
$S_{PS(image)}$					1	0.331 0.194
$S_{PS(PDF)}$						1

* Correlation is significant at the 0.05 level (2-tailed).
** Correlation is significant at the 0.01 level (2-tailed).

Table 7. Pearson's r correlation matrix for the Hurst exponents of four techniques applied: Box dimension, R/S analysis, Power spectrum and Wavelets.

	H_{box} (image)	H_{box} (firmagram)	H_{RS} (image)	H_{RS} (PDF)	H_{PS} (image)	H_{PS} (PDF)	H_w (image)	H_w (PDF)	H_w (firmagram)
$H_{box(image)}$	1	−0.341 0.181	−0.405 0.107	−0.436 0.081	0.446 0.073	−0.414 0.099	0.213 0.412	−0.114 0.664	0.094 0.719
$H_{box(firmagram)}$		1	0.748** 0.001	0.718** 0.001	−0.869** 0.000	0.457 0.065	−0.01 0.969	−0.175 0.501	0.328 0.199
$H_{RS(image)}$			1	0.583* 0.014	−0.674** 0.003	0.608* 0.010	−0.149 0.569	−0.007 0.979	0.004 0.987
$H_{RS(PDF)}$				1	−0.582* 0.014	0.644** 0.005	−0.132 0.614	0.022 0.934	0.463 0.061
$H_{PS(image)}$					1	−0.412 0.100	0.190 0.466	0.022 0.932	−0.246 0.340
$H_{PS(PDF)}$						1	−0.391 0.121	0.130 0.620	−0.128 0.624
$H_{W(image)}$							1	0.140 0.591	0.133 0.610
$H_{W(PDF)}$								1	0.057 0.828
$H_{W(firmagram)}$									1

[*] Correlation is significant at the 0.05 level (2-tailed).
[**] Correlation is significant at the 0.01 level (2-tailed).

Table 8. Pearson's r correlation matrix for the Central moments (raw data) of three studied soils.

	Chernozem	Solonetz	Clay
Chernozem	1	0.99972[**] 0.00028	0.99999[**] 0.00001
Solonetz		1	0.99983[**] 0.00017
Clay			1

[*] Correlation is significant at the 0.05 level (2-tailed).
[**] Correlation is significant at the 0.01 level (2-tailed).

Title Page

Abstract | Introduction

Conclusions | References

Tables | Figures

◄◄ | ►►

◄ | ►

Back | Close

Full Screen / Esc

Printer-friendly Version

Interactive Discussion

Table 9. Student t-test for the Central moments (raw data) of three compared soils.

| | Paired differences | | | | | t | df | Sig. (2-tailed) |
| | Mean | SD | SEM | 95% confidence interval of the difference | | | | |
				Lower	Upper			
Chernozem-Solonetz	252.983	517.124	258.562	−569.876	1075.842	0.978	3	0.400
Chernozem-Clay	−30.430	46.664	23.332	−104.682	43.822	−1.304	3	0.283
Solonetz-Clay	−283.413	562.444	281.222	−1178.387	611.560	−1.008	3	0.388

[*] The differences are significant at the 0.05 level (2-tailed).
[**] The differences are significant at the 0.01 level (2-tailed).

Title Page

Abstract | Introduction

Conclusions | References

Tables | Figures

|◄ | ►|

◄ | ►

Back | Close

Full Screen / Esc

Printer-friendly Version

Interactive Discussion

Table 10. Pearson's r correlation matrix for the Central moments (fit data) of three studied soils.

	Chernozem$_{Fit}$	Solonetz$_{Fit}$	Clay$_{Fit}$
Chernozem$_{Fit}$	1	0.99999** 0.00001	0.99980** 0.00020
Solonetz$_{Fit}$		1	0.99987** 0.00013
Clay$_{Fit}$			1

[*] Correlation is significant at the 0.05 level (2-tailed).
[**] Correlation is significant at the 0.01 level (2-tailed).

Title Page

Abstract | Introduction

Conclusions | References

Tables | Figures

|◄ | ►|

◄ | ►

Back | Close

Full Screen / Esc

Printer-friendly Version

Interactive Discussion

Table 11. Student t-test for the Central moments (fit data) of three studied soils.

	Paired differences					t	df	Sig. (2-tailed)
	Mean	SD	SEM	95% confidence interval of the difference				
				Lower	Upper			
Chernozem$_{Fit}$-Solonetz$_{Fit}$	−50.388	86.680	43.340	−188.316	87.540	−1.163	3	0.329
Chernozem$_{Fit}$-Clay$_{Fit}$	190.321	391.331	195.665	−432.374	813.016	0.973	3	0.402
Solonetz$_{Fit}$-Clay$_{Fit}$	240.709	477.327	238.663	−518.824	1000.242	1.009	3	0.387

[*] The differences are significant at the 0.05 level (2-tailed).
[**] The differences are significant at the 0.01 level (2-tailed).
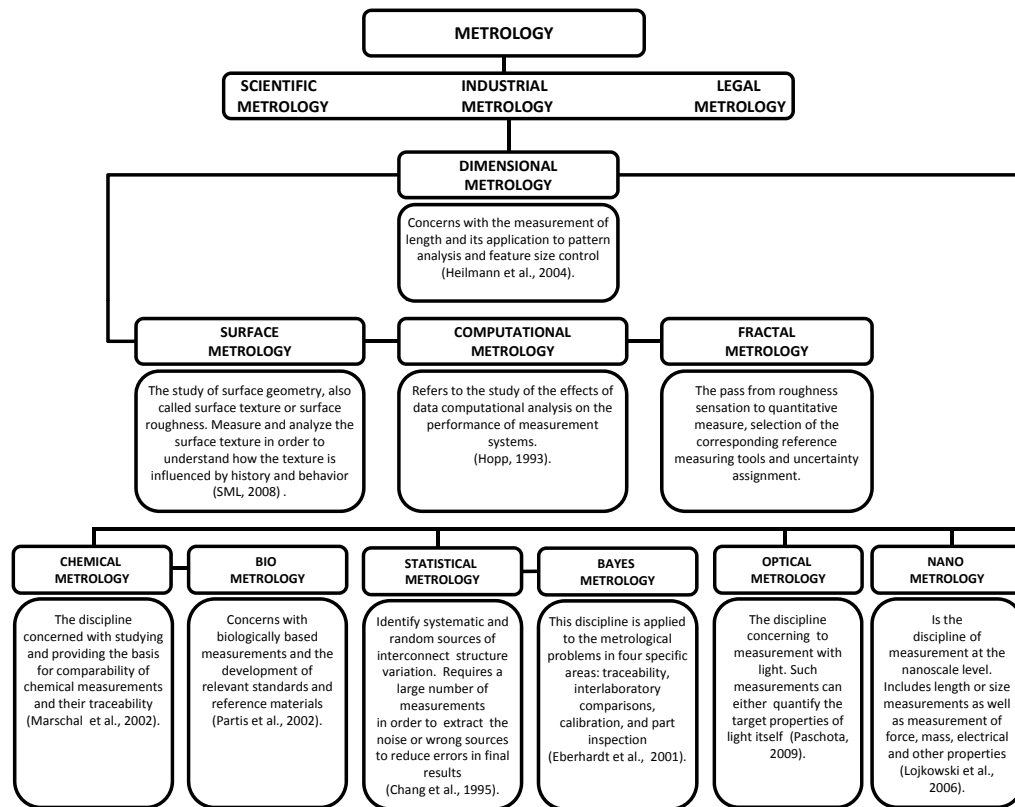
Fig. 1. Metrology division in sub-disciplines.
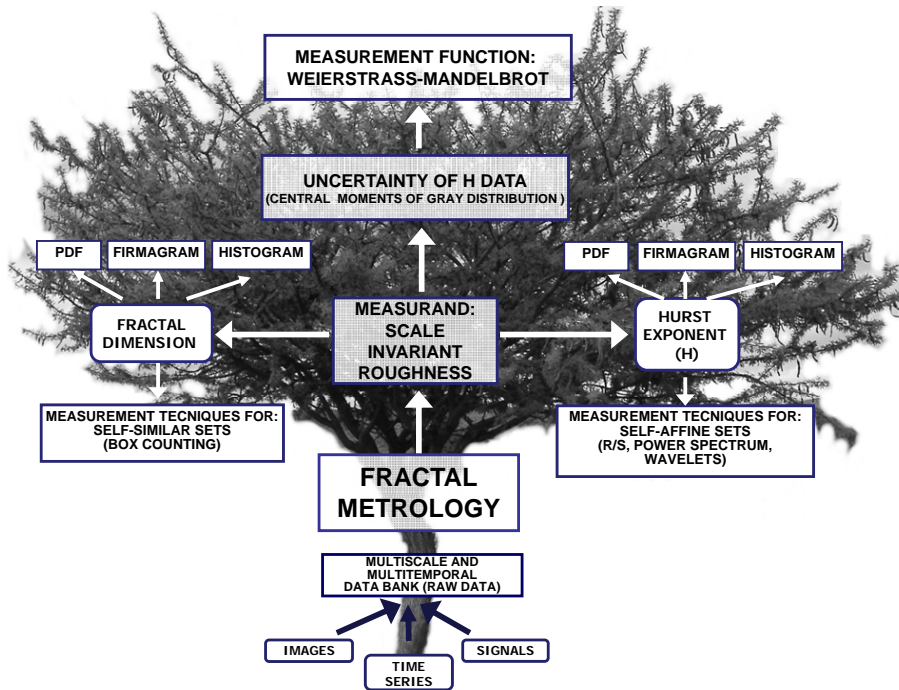
Fig. 2. Hierarchically organized Fractal Metrology construction.

Full Screen / Esc
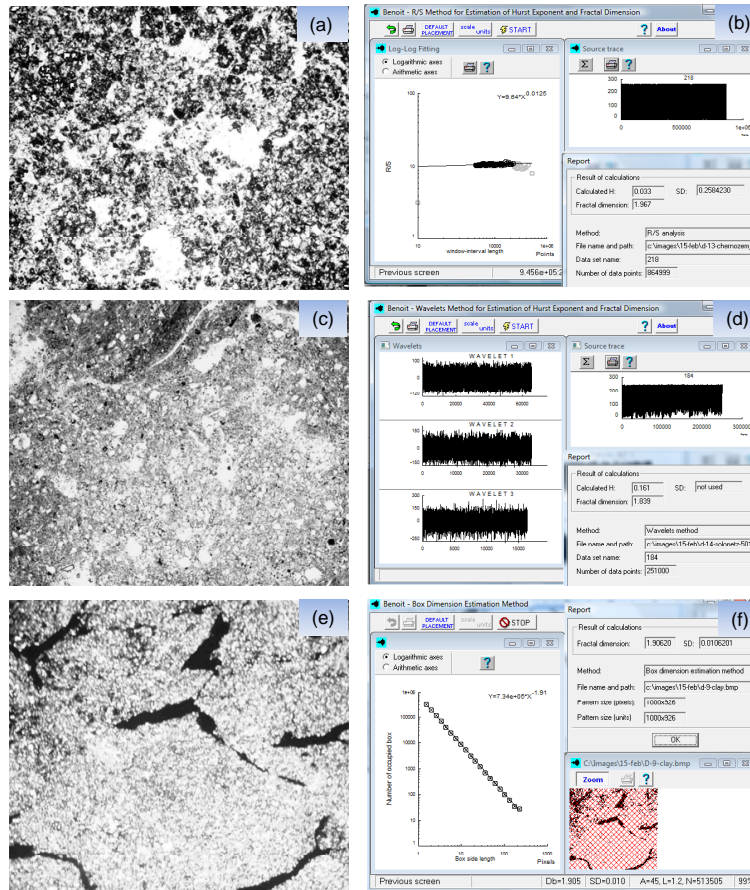
Fig. 3. Benoit (Version 1.3) outputs of the compared methods: R/S analysis **(b)**, wavelets **(d)** and box counting **(e)** applied to images of the Chernozem **(a)**, Solonetz **(c)** and Clay **(e)** visualizing the details of each procedure.

(c)

H_box (image)	H_box (firmagram)	H_RS (image)	H_RS (PDF)	H_RS (firmagram)	H_PS (image)	H_PS (PDF)	H_W (image)	H_W (PDF)	H_W (firmagram)
0.083	0.075	0.021	0.25	0.349	0.27	0.344	0.478	0.564	0.197

(f)

N/A	Fit	Input
Function	#########	N/A
Shift	N/A	N/A
a1	1.16640218	N/A
-a2	0.79032083	N/A
min	0.99247841	N/A
max	255	N/A
N/A	N/A	N/A
Left X	25.1	25.1
Left P	5.00%	4.27%
Right X	250.1	250.1
Right P	95.00%	97.55%
Diff. X	225.0715	225.0715
Diff. P	90.00%	93.28%
Minimum	**0.99248**	**1**
Maximum	**255**	**255**
Mean	**152.41**	**150.8**
Mode	**255**	**245.00 [est]**
Median	**161.95**	**156**
Std. Deviation	**72.483**	**75.216**
Variance	**5253.82**	**5657.43**
Skewness	**-0.3405**	**-0.2115**
Kurtosis	**1.9283**	**1.6916**

(g)

| Sbox (image)	Sbox (firmagram)	SRS (image)	SRS (PDF)	SRS (firmagram)	SPS (imagen)	SPS (PDF)	SPS (firmagram)
0.017	0.002	0.373	0.003	0.115	160194	17.8	57078.05

Fig. 4. Firmagrams **(Ab, Bb, Cb)** extracted from the micromorphological images of three studied soils: Chernozem **(Aa)**; Solonetz **(Ba)** and Clay **(Ca)**, with contrasting structural patterns. The roughness values expressed in terms of Hurst (H) exponent **(Ac, Bc, Cc)** and their standard deviation **(Ag, Bg, Cg)** for the compared techniques. The distributions of gray intensities **(Ad, Bd, Cd)** are identified as visual singularities of image: PDF **(Ad, Bd, Cd)**. These differences are detectable by eye when the graphs of data are fitted to the most probable theoretical distribution by software @Risk **(Ae, Be, Ce)**, and with the central moments calculated by the same software **(Af, Bf, Cf)**.

(B)
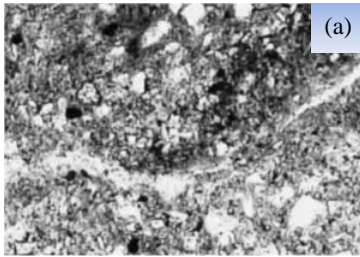
(a)
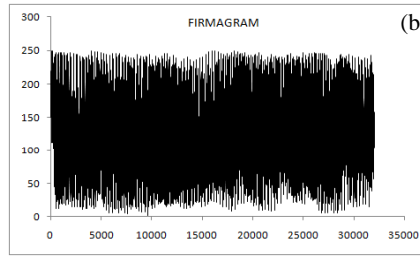
(b) FIRMAGRAM

H$_{box}$ (image)	H$_{box}$ (firmagram)	H$_{RS}$ (image)	H$_{RS}$ (PDF)	H$_{RS}$ (firmagram)	H$_{PS}$ (image)	H$_{PS}$ (PDF)	H$_W$ (image)	H$_W$ (PDF)	H$_W$ (firmagram)	(c)
0.107	0.092	0.035	0.426	0.199	0.231	0.47	0.161	0.209	0.464	

N/A	Fit	Input	(f)
Function	##########	N/A	
Shift	N/A	N/A	
a1	2.09339997	N/A	
-a2	1.62733436	N/A	
min	0.93896285	N/A	
max	251.107105	N/A	
N/A	N/A	N/A	
Left X	43.7	43.7	
Left P	5.00%	4.34%	
Right X	229.3	229.3	
Right P	95.00%	93.27%	
Diff. X	185.5623	185.5623	
Diff. P	90.00%	88.93%	
Minimum	**0.93896**	**1**	
Maximum	**251.11**	**251**	
Mean	**141.69**	**140.93**	
Mode	**159.9**	**240.00 [est]**	
Median	**144.76**	**140**	
Std. Deviation	**57.117**	**56.767**	
Variance	**3262.32**	**3222.4**	
Skewness	**-0.1918**	**-0.062**	
Kurtosis	**2.1542**	**2.1802**	
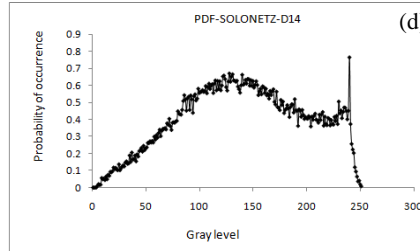
(d) PDF-SOLONETZ-D14
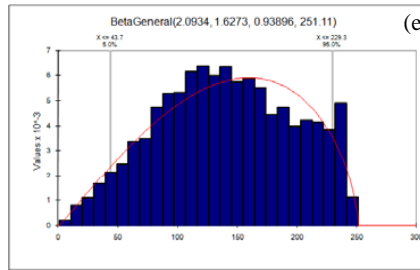
(e) BetaGeneral(2.0934, 1.6273, 0.93896, 251.11)

Sbox (image)	Sbox (firmagram)	SRS (image)	SRS (PDF)	SRS (firmagram)	SPS (imagen)	SPS (PDF)	SPS (firmagram)	(g)
0.015	0.006	0.294	0.005	0.1	147173	11.5	34694.45	

Fig. 4. Continued.

(C)

(a)
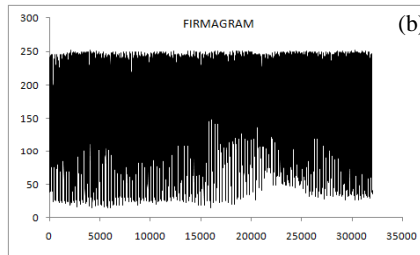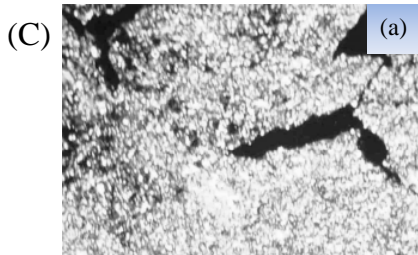
FIRMAGRAM (b)

H_box (image)	H_box (firmagram)	H_RS (image)	H_RS (PDF)	H_RS (firmagram)	H_PS (image)	H_PS (PDF)	H_W (image)	H_W (PDF)	H_W (firmagram) (c)
0.094	0.156	0.025	0.508	0.088	0.126	0.276	0.526	0.601	0.724

N/A	Fit	Input (f)
Function	#########	N/A
Shift	N/A	N/A
a1	2.81835131	N/A
-a2	246	N/A
min	253.07713	N/A
max	N/A	N/A
N/A	N/A	N/A
Left X	58	58
Left P	5.00%	8.67%
Right X	243.3	243.3
Right P	95.00%	94.03%
Diff. X	185.2857	185.2857
Diff. P	90.00%	85.36%
Minimum	**2.8184**	**15**
Maximum	**253.08**	**253**
Mean	**167.3**	**176.84**
Mode	**246**	**240.00 [est]**
Median	**177.26**	**194**
Std. Deviation	**58.17**	**62.203**
Variance	**3383.8**	**3869.12**
Skewness	**-0.5641**	**-0.9822**
Kurtosis	**2.4**	**2.986**
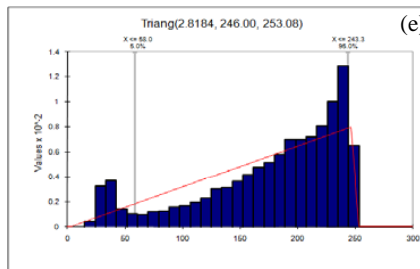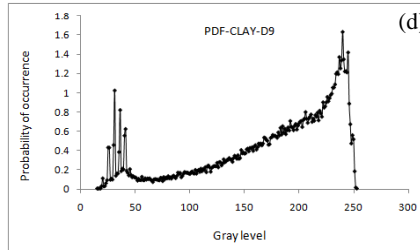
PDF-CLAY-D9 (d)

Triang(2.8184, 246.00, 253.08) (e)

Sbox (image)	Sbox (firmagram)	SRS (image)	SRS (PDF)	SRS (firmagram)	SPS (imagen)	SPS (PDF)	SPS (firmagram) (g)
0.01	0.002	.493	.004	.065	155004.67	4.3	32958.29

Fig. 4. Continued.